A CONSTANT CRITICAL COUPLING COEFFICIENT CONTROL METHOD FOR WIRELESS POWER TRANSFER SYSTEMS UNDER VARIABLE LOAD

Jun WU[1], Hongping XIE[2], Jun KONG[3], Chao HAN[4], Ke SUN[5], Zhiwei LIU[6], Sugang LI[7*], Youkang WANG[8], Chaoran YANG[9], Shiqing ZHANG[10]

Fluctuations of critical coupling coefficient in parity-time (PT) symmetric wireless power transfer (WPT) systems have significant influences on their transfer performance. To solve this problem, this research proposed a method based on power electronic topology to stabilize its transfer performance. Firstly, a mathematical model was established based on two-coil magnetically coupled resonant wireless power transfer (MCR-WPT) topology of the series-series (S-S) type in a stable state. The formulation of the critical coupling coefficient of the system was derived considering stable state. Then, a control approach based on output-end Buck-Boost converter was designed, which could be applied for the stabilization of the critical coupling coefficient of the system. This approach ensured that the system could provide a stable PT-symmetric solution space under variable loads. Finally, a WPT system was designed, boasting transfer efficiency of 80% and output power of 40W. The transfer characteristics of the system under load perturbation was verified using simulation and experiment. Research results demonstrated that the proposed method could retain the system with constant critical coupling coefficient and stable output power and transmission efficiency under load disturbance.

Keywords: load perturbation, dynamic wireless power transfer system, critical coupling coefficient, Parity-time symmetry, magnetically coupled resonant

1. Introduction

Wireless power transfer (WPT) has several advantages, including safety, convenience, and robustness. Non-contact nature of power transfer process renders it suitable for applications in specialized charging locations where safety and

[1] Yangtze River International Shipping Centre, China, e-mail: carrezyuillc70e@hotmail.com
[2] Yangtze River International Shipping Centre, China
[3] Yangtze River International Shipping Centre, China
[4] Yangtze River International Shipping Centre, China
[5] Yangtze River International Shipping Centre, China
[6] Yangtze River International Shipping Centre, China
[7] * Xi'an Jiaotong University, Xi'an, Shaanxi 710049, China, corresponding author, e-mail: 3123104279lisugang@stu.xjtu.edu.cn
[8] Xi'an Jiaotong University, Xi'an, Shaanxi 710049, China
[9] Xi'an Jiaotong University, Xi'an, Shaanxi 710049, China
[10] Xi'an Jiaotong University, Xi'an, Shaanxi 710049, China

convenience are critical [1]. In recent years, WPT systems have become very popular in various applications, including portable electronics, electric vehicles, and biomedical implants. However, complex load characteristics during the charging process of these electronic devices impose high requirements on WPT system designs, not only the perturbation of coil coupling coefficient, but also the role of impedance perturbation at load side should be considered in the designed systems [2].

In a medium-range WPT system consisting of a magnetically coupled resonant WPT, coil coupling coefficient perturbation and load impedance parameter perturbation cooperate to affect the overall transfer characteristics of the system [3,4]. To address this problem, Sid et al. designed a WPT system with stable transfer performance within a certain coil coupling coefficient range [5]. They introduced the concept of parity-time (*PT*) symmetry into WPT system and used operational amplifiers to construct a power supply gain proportional to the load loss, such that the developed system demonstrated consistent power transfer efficiency and stable output power across a wide coupling coefficient range [6]. However, due to the limitations of operational amplifiers themselves, it was difficult to enhance the maximum transfer power and transfer efficiency of the system. To solve this problem, Hua et al. developed a high-power WPT system that was resilient to the perturbations of coupling coefficient [7]. They did this by developing a power supply gain using half-bridge and full-bridge topologies. These research works adequately addressed the influences of coil coupling coefficient perturbation on transfer performance. In practical applications, load impedance perturbation also significantly affected system transfer performance, which in turn influenced system design [8-10].

To solve the problem reduction and fluctuation in the power delivery and efficiency performance of each system link due to load disturbance, researchers have developed several tracking control approaches [11]. For example, Luo et al. applied frequency tracking control to MCR-WPT systems using a DSP (Digital Signal Processing) to operate the system at maximum transfer efficiency point [12-14]. However, this control method only searched for better working points on the existing solution space and did not regulate the system solution space itself.

In this research, we analyzed the topology of series-series (S-S) type two-coil WPT systems and solved its stable-state solution space. This research successfully identified the PT-symmetric operating point of the system, which maintained consistent power delivery and efficiency maintenance. To realize system stability, a Buck-Boost converter was implemented to regulate the critical coupling coefficient. This configuration ensured the preservation of stable PT-symmetric characteristics at different load resistances, thereby guaranteeing sustained operational performance of both power delivery and efficiency maintenance.

2. Theoretical analysis

S-S type two-coil topology is one of the four commonly applied structures in MCR-WPT systems. This system has a simple structure and good transfer characteristics over medium distances. Fig. 1 shows the equivalent circuit. In the figure, U_{in} is high-frequency excitation power supply for S-S type topology, M is the mutual inductance of the coil, R_L is load resistor, R_T and R_R are the internal resistances of transmitting and receiving coils, C_T and C_R are capacitance at transmitting and receiving ends, and L_T and L_R are the inductance of transmitter and receiver, respectively.

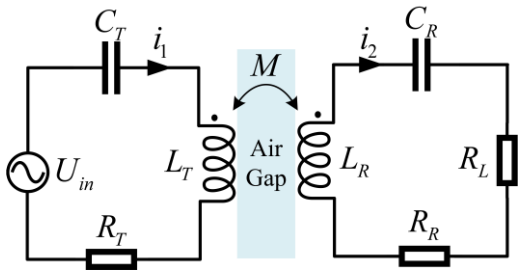

Fig. 1. Equivalent circuit of S-S type PT-symmetric WPT topology

The stable-state model of the circuit for the system depicted in Fig. 1 was stated as follows:

$$\begin{bmatrix} U_{in} \\ 0 \end{bmatrix} = \begin{bmatrix} Z_T & j\omega M \\ j\omega M & Z_R \end{bmatrix} \begin{bmatrix} I_T \\ I_R \end{bmatrix} \tag{1}$$

where I_T and I_R are loop currents of transmitter and receiver sides, respectively, $Z_T = R_T + j\omega L_T + 1/j\omega C_R$, $Z_R = R_R + R_L + j\omega L_R + 1/j\omega C_R$, and U_{in} is the root-mean-square (RMS) value of the output voltage of the high-frequency AC excitation power supply. The transmission characteristics of the system were determined by solving loop stable state equations. They were plotted at different coupling coefficients and operating frequencies ω in Fig. 2.

The minimum points in coupling coefficients corresponding to the red lines in Figs. 2 are the critical coupling points. The point where the coupling coefficients exceeded the critical coupling coefficients were defined as system *PT*-symmetric region. The PT-symmetry broken region is conversely defined. The red curve in the figure corresponds to the system's PT-symmetric operating point. It can be observed that at this point, the output power, transfer efficiency, and equivalent input impedance remain constant. This stability is crucial for ensuring reliable system operation, with their specific values as follows:

$$\begin{cases} P_o = U_{in}^2 R_L \big/ \left(R_T + R_R + R_L\right)^2 \\ \eta = R_L / (R_T + R_R + R_L) \\ Z_{eq} = R_T + R_R + R_L \end{cases} \tag{2}$$

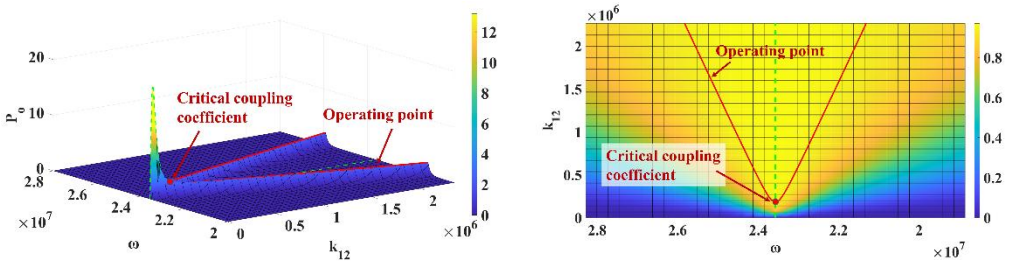

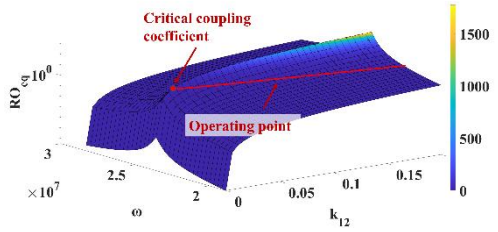

Fig. 2. Analysis of System Transmission Characteristics. (a) Variations of output power with coupling coefficient and operating frequency. (b) Variations of transfer efficiency with coupling coefficient and operating frequency. (c) Variations of system equivalent input impedance with coil coupling coefficient and system operating frequency

As shown in Fig. 2, when the system crosses the boundary of the symmetric region (i.e., $k_{12} < k_c$), it no longer possesses a stable operating point. It is therefore necessary to control the boundary of the symmetric region to ensure the stability of the system's symmetric interval under disturbances. The relationship between operating angular frequency and coupling coefficient within the symmetric region was described as:

$$\omega = \frac{\omega_0^2 - 2\Gamma_2^2}{1-k_{12}^2} \pm \sqrt{\frac{[\omega_0^2 - 2\Gamma_2^2]^2}{\left(1-k_{12}^2\right)^2} - \frac{1}{1-k_{12}^2}\omega_0^4} \tag{3}$$

where:

$$\Gamma_2 = \frac{R_R + R_L}{2L} \tag{4}$$

As described in Eq. (3), when the coupling coefficient k_{12} was larger than the critical coupling coefficient k_c, the system had two working solutions of high

frequency and low frequency and when $k_{12} = k_c$, the high-frequency and low-frequency working solutions overlapped. Thus, the value of k_c can be obtained as:

$$k_c = \sqrt{1-[1-\frac{1}{2}(\frac{R_R + R_L}{\omega_0 L_2})^2]^2} \tag{5}$$

k_c revealed relationships with load resistance R_L, equivalent resistance of the receiving-side circuit, intrinsic operating frequency of the magnetically coupled resonator and coil inductance. After the system was designed, all other parameters remained fixed except for R_L. When R_L was increased, *PT*-symmetric operating solution curve was drawn, as illustrated in Fig. 3.

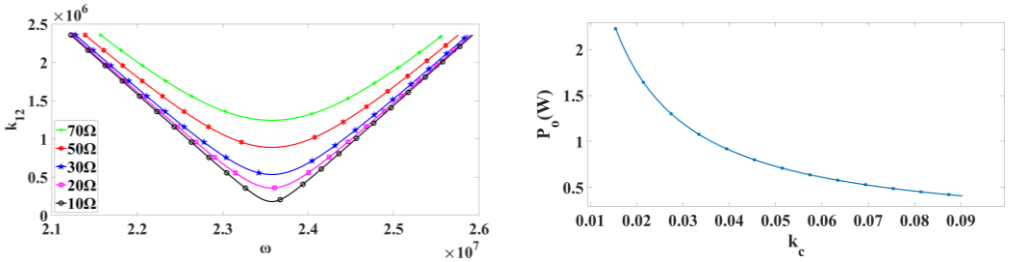

(a) (b)

Fig. 3. Impact of Load Resistance on Transmission Characteristics. (a) PT-symmetric solution of the system with load resistance. (b) System output power with k_c.

As presented in Fig. 3(a), increase of load resistance corresponded with in the increase of k_c, which in turn decreased the PT-symmetric region. With the increase of load resistance from 10 to 70 Ω, PT-symmetric interval was decreased by about 50%, substantially decreasing the perturbation-resistant capacity of the coil. Fig. 3(b) shows the variations of output power within PT-symmetric zone as a function of k_c. With the increase of k_c, output power in the symmetric interval was dramatically decreased, thus affecting the stable operation of the system.

3. Topology and realization

Relying on soft-switching characteristics during operation, class E power amplifiers can reduce system switching loss during high-frequency operations, thereby enhancing system efficiency. This chapter investigates the control scheme for an S-S type WPT system driven by a Class E amplifier. First, a buck-boost converter topology is introduced at the system output. This achieves stable control of the k_c under varying load conditions, thus maintaining the stability of the system's solution space. Subsequently, a closed-loop control method is presented that automatically adjusts the system to the PT-symmetric point. This enables the system to stabilize at the PT-symmetric point within the solution space.

The system topology diagram incorporating the back-end DC-DC converter is shown in Fig. 4. When the system shown in Fig. 4 operates at the PT operating point, the equivalent resistance of the loaded network is expressed as:

$$R_{eq} \approx R_{eq}^{'} \tag{6}$$

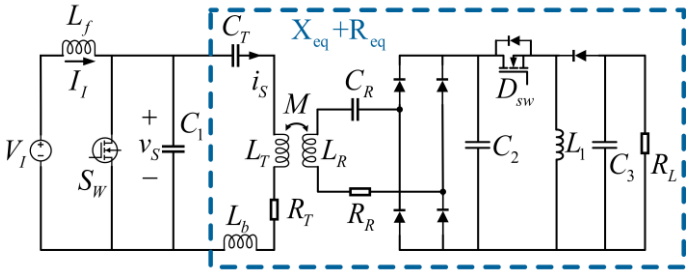

Fig. 4. Topology of WPT system using DC-DC series modulation

Where R'_{eq} is the equivalent resistance of the circuit connected to the secondary resonator. To ensure the stabilization of the system's PT-symmetric solution space and the efficient operation of the Class E power amplifier, the Buck-Boost circuit's impedance transformation characteristic must be leveraged to achieve the stability value $R'eq = R'opt$. $R'opt$ represents the optimum impedance for the Class E power amplifier at the system's natural operating frequency. The equivalent impedance at the input and output ports of the Buck-Boost circuit exhibited a specific relationship, stated as:

$$R_{in} = R_{out}(\frac{1-D}{D})^2 = R_L(\frac{1-D}{D})^2 \tag{7}$$

The correlation of equivalent impedances at source and load ports in full-bridge rectifier was expressed as [15]:

$$R_{in} = R_{opt}^{'} = \frac{8}{\pi^2} R_{out} \tag{8}$$

For any load resistance R_L, considering the relationship between the input impedance and the output impedance of the full-bridge uncontrolled rectifier, the duty cycle of the switch tube in the Buck-Boost topology should be adjusted as follows:

$$D = \frac{1}{1+\sqrt{\frac{\pi^2 R_{opt}^{'}}{8R_L}}} \tag{9}$$

The closed-loop control scheme for tracking the PT-symmetric point is presented below. Fig. 5 illustrates the relationship between the current phase angle

φ in the Class E amplifier's load network and the real/imaginary components of the load network impedance.

With horizontal and vertical coordinates being the normalized values of resistance and reactance in the load network, respectively, and the transfer efficiency of the system reaching its maximum value when the system satisfied both ZVS and ZDS operating conditions when $X_{eq} = X_{opt}$, $R_{eq} = R_{opt}$, X_{opt} and R_{opt} were expressed as:

$$X_{opt} = \frac{\pi(\pi^2 - 4)}{16} R_{opt} \tag{10}$$

$$R_{opt} = \frac{8}{\pi(\pi^2 + 4)\omega C_1} \tag{11}$$

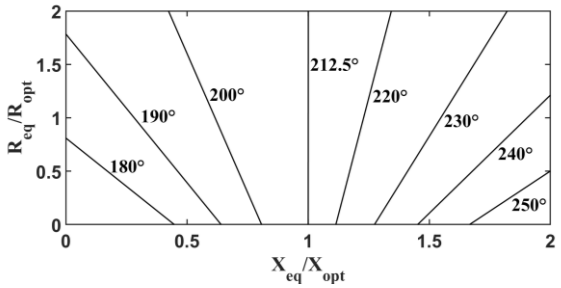

Fig. 5. Variations of current phase with real and imaginary parts of the load network

As shown in Fig. 5, the reactance value of the load network was constant at X_{opt} when load network current was 212.5°. For the load network consisting of residual inductance L_b and S-S type MCR-WPT topology, operating point distribution with reactance values equal to X_{opt} throughout the operating region is presented by the blue curves in Fig. 6.

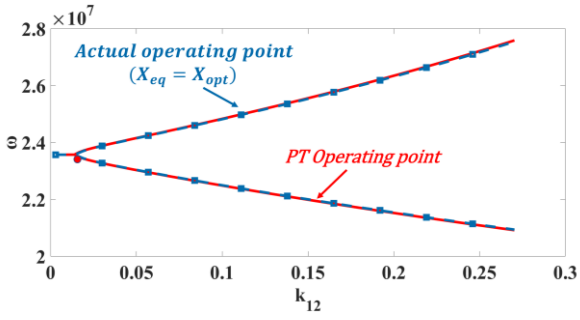

Fig. 6. Distribution of operating points at $X_{eq} = X_{opt}$ for S-S type WPT system

As illustrated in Fig. 6, the operating curve of the load network exhibited a high degree of congruence with the *PT*-symmetric operating curve of S-S type topology when satisfying $X_{eq} = X_{opt}$. Therefore, the system can operate at the PT

symmetric point by keeping the operating phase angle of load network currents constant at 212.5°. By integrating this with the aforementioned control of Req, the Class E amplifier can thus operate in soft-switching mode.

The constant phase angle controller can be implemented by the circuit shown in Fig. 7. Voltage signal was sampled by the detection coil located on the transmitter side, isolated by voltage follower, fed into RC phase-shift circuit, and then, shifted by phase-shift circuit by 122.5°. Finally, phase-shifted sinusoidal waveform was converted into a square-wave control signal by comparator for class E amplifier switching tubes and fed into the drivers of switching tubes.

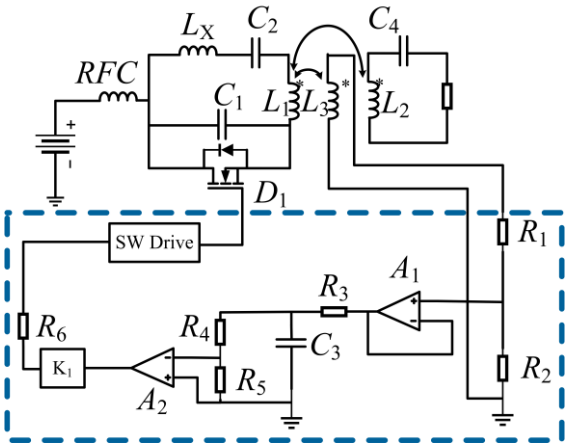

Fig. 7. The schematic diagram of current closed-loop controller on the launch side

The proposed circuit topology and closed-loop control method provided a stable *PT*-symmetric solution space for the system under fluctuating loads and coupling coefficients. At the same time, the system was capable of self-stabilizing to PT-symmetric solution within the solution space, ensuring consistent power delivery and efficiency performance.

4. Experimental verifications

Based on the above analyses, experimental verifications were performed in this section to evaluate the performance of the designed circuit topology and the operation of the closed-loop control structure.

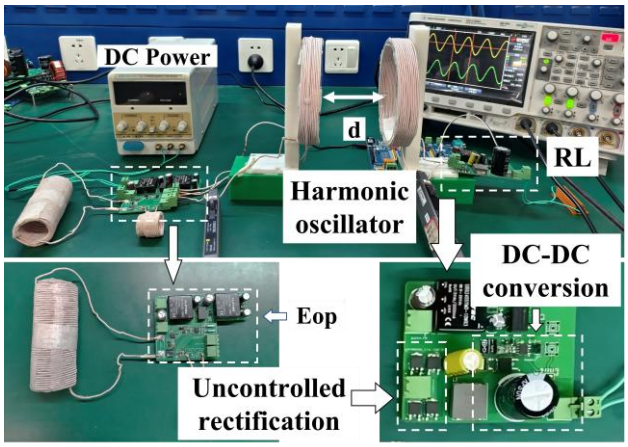

Fig. 8. The developed experimental platform

Fig. 8 shows the developed experimental prototype, where the power was emitted from a DC source, inverted into high-frequency alternating current by a class E power amplifier, fed into the transmitting side of the magnetically coupled resonator, a full-bridge uncontrolled rectifier and a DC-DC converter connected to the receiving side, and finally flew into the load resistor. To obtain high-frequency operation of class-E power amplifiers, GaN device GS6650 was employed as switching tube. The GS6650 is an enhancement-mode gallium nitride (GaN) power transistor designed for high-frequency operation. For the magnetically coupled resonator, to minimize losses due to high-frequency skin effect and dielectric dissipation, Litz wire (ϕ 0.05 mm × 660 strands, OD 1.83 mm) was applied to wind the magnetically coupled resonator coil. At the receiver, full-bridge rectifier utilized Schottky diodes (FERD20H100SB) with low on-resistance, while DC-DC converter employed a lift-voltage topology converter (MOSFET: GS66508B, current-continuing diode: FERD20H100SB).

The values of the system parameters are shown in the Table I.

Table I

System parameter

Name of parameter	Parameter values
Choke inductor L_f (μH)	300
Residual inductor L_b (μH)	4.236
switching tube shunt capacitance C_1 (nF)	6.75
angular frequency ω_0 (MHz)	2.72
Resonant inductor L (μH)	134.86
Resonant capacitor C (nF)	1
Direct voltage V_1 (V)	29.442

Firstly, the prototype was tested under different loads and coupling coefficients to verify the transmission characteristics analyzed above. Figs. 9 illustrate the k_c, output power characteristics, and efficiency performance of the system under varying load conditions.

Under the action of DC-DC converter, system k_c could be kept constant under variable load resistance R_L; simultaneously, the output power stability was significantly increased compared to the circuit without DC-DC converter, which was in line with the theoretical design. The efficiency of the system in transmission remained stable despite the variation of load resistance to a large extent. Due to the existence of harmonic oscillator equivalent series resistance, the overall working efficiency of only about 80% could be obtained.

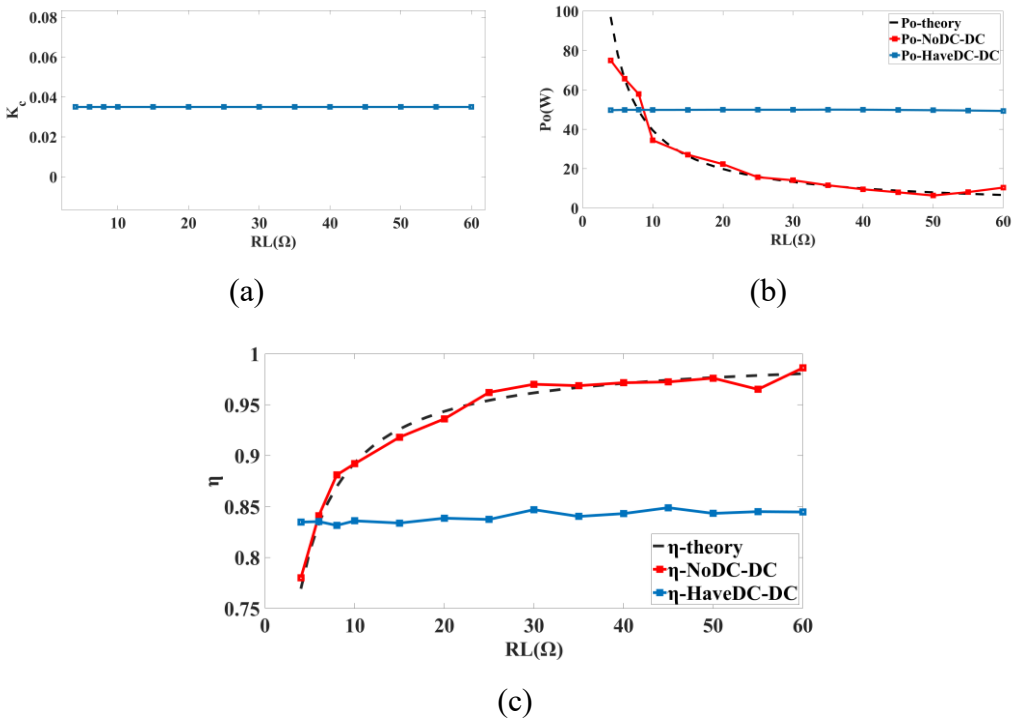

Fig. 9. Analysis of Experimental Results. (a) Variation of kc with load resistance. (b) Variation of output power with load resistance RL. (c) Variation of transfer efficiency with load resistance.

Fig. 10 shows the relationship between the operating frequency and coupling coefficient. 2.4, 4.8 and 10 Ω load resistances were selected for the experiment and accordingly, the variation of the working frequency with the coupling coefficient was measured. The measurement results indicated that the PT symmetric solution space was no longer affected by the change of the load resistance R_L. Among them, in experimental test with $R_L = 10\Omega$, the operating point of the system alternated between high-frequency and low-frequency branches under

large coupling coefficients, but the system could still maintain a high transfer efficiency and output power due to the symmetry of transfer characteristics on high-frequency and low-frequency branch curves in PT-symmetric region.

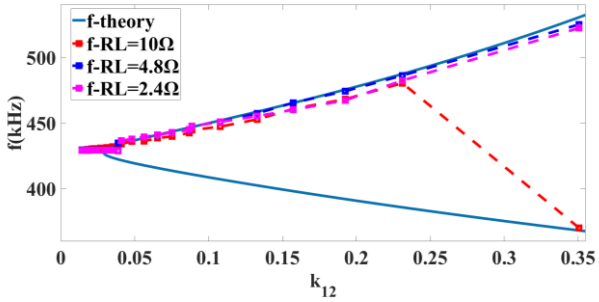

Fig. 10. Variations of system operating frequency with coil coupling coefficient for different load resistances

5. Conclusions

This research introduced a WPT system based on PT-symmetric principles, featuring stabilized critical coupling characteristics. The quantitative relationship between the k_c and transfer characteristics of the system was determined by analyzing the mathematical model of the two-coil MCR-WPT topology of the series-series (S-S) type in a stable state. It was found that increase of k_c decreased the transfer efficiency and output power of the system with an exponential multiplication rate, which was important to keep system k_c constant for stable operation. Therefore, the relationship between load resistance R_L and *PT*-symmetric radio power transfer system solution space was evaluated. It was found that k_c and the position of solution space could be changed by adjusting R_L. Then, an approach was proposed based on lifting voltage converter at output. The purpose of this approach was to stabilize and control two elements: system k_c and its symmetric solution space. Following a rigorous testing process on the constructed simulation and physical models, it was shown that the power delivery and efficiency performance of the system by adding DC-DC impedance stabilizer exhibited enhanced stability under variable loads. This finding signified that the system could effectively improve the application of electronic devices with changing loads.

Acknowledgement

This work was supported by State Grid Jiangsu Electric Power Engineering Consulting Co., Ltd. Science and Technology Project (J202309).

REFERENCES

[1] Tan C., Design and Implementation of E-Class Power Amplifier for Magnetic Coupling Resonant Wireless Power Transfer; Nanjing University of Science and Technology, 2017.
[2] Hou Y, Lin M, Chen W, et al., Parity-time-symmetric Wireless Power Transfer System Using Switch-mode Nonlinear Gain Element//2018 IEEE International Power Electronics and Application Conference and Exposition (PEAC), 2018: 1-5.
[3] Li C, Dong W, Ding L, et al., Transfer Characteristics of the Nonlinear Parity-Time-Symmetric Wireless Power Transfer System at Detuning, 2020, 13(19):10.3390/en13195175
[4] Aldhaher S, Yates D C, Mitcheson P D., Design and Development of a Class EF$_2$ Inverter and Rectifier for Multimegahertz Wireless Power Transfer Systems. IEEE Trans Power Electron, 2016, 31(12): 8138-8150.
[5] Sid A, Xiaofang Y, Shanhui F., Robust wireless power transfer using a nonlinear parity-time-symmetric circuit. . Nature, 2017, 546(7658): 387-390.
[6] Chen P, He S., Analysis of Inverse Class-E Power Amplifier at Subnominal Condition With 50% Duty Ratio. IEEE Transactions on Circuits and Systems II: Express Briefs, 2015, 62(4): 342-346.
[7] Hua Z, Chau K T, Liu W, et al., Autonomous Pulse Frequency Modulation for Wireless Battery Charging With Zero-Voltage Switching. IEEE Trans Ind Electron, 2023, 70(9): 8959-8969.
[8] Liu G, Zhang B., Dual-coupled robust wireless power transfer based on parity-time-symmetric model. Chinese Journal of Electrical Engineering, 2018, 4(2): 50-55.
[9] Zhou J L, Zhang B, Xie F., Analysis of E-Class Inverter Circuit in Magnetic Resonant Wireless Power Transfer System . Journal of Beijing Jiaotong University, 2015, 39(5): 112-117.
[10] Yang J Y., Research on Efficiency Stability of Tri-Coil Wireless Power Transfer System Based on E-Class Power Amplifier; Nanjing Normal University, 2020.
[11] Du C S, Chen C Y, Liu Z F, 1.8GHz CMOS High-Efficiency E-Class Power Amplifier . Semiconductor Technology, 2007, 32(8): 4.
[12] Li J F, Liao C L, Wang L F., Medium-Range Wireless Power Transfer System Based on E-Class Amplifier .Transactions of China Electrotechnical Society, 2014, 29(09): 7-11.
[13] Luo J, Shen H, Xu X., DSP-based adaptive digital control method for frequency tracking and impedance angle control of MCR–WPT systems. Journal of Power Electronics, 2024, 25(3): 1-10.
[14] Zhu H, Zhang B, Wu L., Output Power Stabilization for Wireless Power Transfer System Employing Primary-Side-Only Control. IEEE Access, 2020, 8: 63735-63747.
[15] Wang P F., Design and Research of Magnetic Coupling Resonant Wireless Power Transfer System Based on PT Symmetry; Shenyang University of Technology, 2022.